The power of joint application of LEED and DFT in quantitative surface structure determination

2008 J. Phys.: Condens. Matter 20 304204

(http://iopscience.iop.org/0953-8984/20/30/304204)

J. Phys.: Condens. Matter **20** (2008) 304204 (9pp) doi:10.1088/0953-8984/20/30/304204

The power of joint application of LEED and DFT in quantitative surface structure determination

K Heinz, L Hammer and S Müller

Lehrstuhl für Festkörperphysik, Universität Erlangen-Nürnberg, Staudtstraße 7, D-91058 Erlangen, Germany

E-mail: klaus.heinz@physik.uni-erlangen.de

Received 5 November 2007, in final form 9 January 2008
Published 8 July 2008
Online at stacks.iop.org/JPhysCM/20/304204

Abstract

It is demonstrated for several cases that the joint application of low-energy electron diffraction (LEED) and structural calculations using density functional theory (DFT) can retrieve the correct surface structure even though single application of both methods fails. On the experimental side (LEED) the failure can be due to the simultaneous presence of weak and very strong scatterers or to an insufficient data base leaving different structures with the same quality of fit between experimental data and calculated model intensities. On the theory side (DFT) it can be difficult to predict the coverage of an adsorbate or two different structures may own almost the same total energy, but only one of the structures is assumed in experiment due to formation kinetics. It is demonstrated how in the different cases the joint application of both methods—which yield about the same structural precision—offers a way out of the dilemma.

1. Surface structure determination

As commonly accepted, knowledge of the crystallographic structure of a surface is essential for the quantitative understanding of most issues in surface science. As a consequence, surface scientists have always aimed to retrieve this structure and a number of different methods have been developed in the last 40 years or so. According to the statistics of the current version of the Surface Structure Data Base [1], of which Sir John Pendry was one of the initiators [2], quantitative low-energy electron diffraction (LEED) has always been the dominant method of structure determination. Even today with the availability of methods as competitive as surface x-ray diffraction (SXRD) LEED appears to be still in the lead. This is in spite of the method's high computational demands as caused by the strong multiple scattering of electrons. It seems to be due, at least partly, to the fact that the technique can be applied in any laboratory with no need to use dedicated sources. Also, with the arrival of the scanning tunnelling microscope (STM) many structural model types can be discarded which would otherwise have to be tested in the analysis in accounting for the symmetry of the observed diffraction pattern. This makes the LEED analysis easier, and explains why the application of atomically resolved STM in parallel to LEED is frequently used and highly recommended [3].

Yet as any single method LEED has its drawbacks too. It is difficult to detect weakly scattering atoms in the presence of other strong scatterers so that, as an example, the adsorption sites of hydrogen on a metal surface can be determined only in exceptional cases [4, 5]. Also, atoms scattering similarly (e.g. when they are neighbours in the periodic table of elements) can be hardly distinguished so that, as an example, intermixing in the epitaxial system of Ni and Cu cannot be tested [6]. Yet there is an even more serious drawback which is not restricted to special cases: even when the correct type of a structural model is identified, the determination of the numerical values of its various structural parameters, by which the model is quantitatively described, can be rather demanding. This is particularly so when there is a large number of such parameters, say in the range 20–100. Then any procedure to fit the calculated model intensities to the experimental data—which is usually controlled by so-called reliability factors (*R*-factors), in particular the widely used Pendry *R*-factor [7]—runs the risk of ending in a local minimum of the *R*-factor hypersurface rather than the global one. Though sophisticated structural search methods have been developed, as for instance genetic [8] or simulated annealing [9] algorithms (see also the review [10] and the paper by Blanco-Rey *et al* in the present volume), the risk is always there. A frequently recommended way out of this dilemma is the parallel application of at least

another structure-sensitive experimental method or, possibly, spin-polarized LEED which gives additional information, in particular when magnetic surfaces are involved. When this leads to the same structure as found by LEED it can rather safely be assumed that the retrieved minimum of the R-factor is global.

However, the parallel application of two or more experimental methods is tedious and might even not help to identify weak scatterers or distinguish between similar ones. Instead, the combination of quantitative LEED with a theoretical method such as total energy calculations by density functional theory (DFT) offers a high chance of determining the full and correct structure. DFT does not just heal the shortcomings of LEED by identifying the correct structure according to the calculated minimum energy and by adding the structural features to which LEED is more or less insensitive: DFT just identifies which structure parameters within a certain class of structure own the lowest energy—no matter whether or not this class meets the experimental situation. It might also be uncertain in the sense that two (or more) different structures are—within the accuracy of the method—energetically degenerate with only one of them realized in the experiment, possibly stabilized by surface kinetics. Then LEED has the potential to identify this structure among those that are degenerate in the calculation. The present paper demonstrates the power of this interplay between LEED and DFT by presenting a selection of examples.

2. Basics of experiments and computations

The LEED experiments for the surfaces presented below were carried out for normal incidence of the primary beam and the sample held at liquid air temperature. The intensity data were collected by use of a digital TV camera which viewed the full LEED pattern from outside the ultra-high vacuum vessel and stored it on a hard disk at a preselected and equidistant grid of energies (0.5 eV step width). From this series of frames the intensity versus energy spectra, $I(E)$, were produced for each beam by computer controlled integration of the stored video signal across the beam with background subtraction applied. Eventually, all spectra were normalized with respect to the primary beam current which had been measured in parallel (for more details of the method see [10, 11]).

The dynamical scattering of the electrons in model structures was calculated using the TensorLEED method [11–13] with the TensErLEED code [14] applied. The method starts with the full dynamical calculation of the intensities for a certain reference structure whereby the usual hierarchical procedure is applied: first the atomic phase shifts are calculated, then the multiple scattering within an atomic layer is computed self-consistently by matrix inversion and eventually the scattering of the full surface is determined by stacking the layers by the layer doubling method [15]. In a second step the resulting intensities of the reference intensities undergo a perturbation calculation by which the intensities of the structures close to the reference structure can be computed.

Comparison of the computed model spectra is made by the Pendry reliability factor (R-factor) which today is the most commonly used [7]. Special values of it are 0, 1 and 2 for identical, fully uncorrelated and fully anticorrelated spectra, respectively. For the search of the best-fit structure within the parameter space given we applied a frustrated simulated annealing procedure described in detail elsewhere [9]. For the estimation of error limits the variance of the R-factor, $\mathrm{var}(R) = R\sqrt{8V_{0i}/\Delta E}$, is applied with V_{0i} the optical potential to simulate electron attenuation and ΔE the total energy width of the data base as accumulated from all beams measured. (In case of an energy dependent V_{0i} its energy-averaged value is used.)

The DFT results presented below were calculated using the Vienna *ab initio* simulation package (VASP [16, 17]). Here, the application of ultrasoft pseudopotentials [18, 19] and, more recently, so-called PAW (projector augmented wave) potentials [20, 21] allow for an accurate and fast treatment of many systems by a plane-wave basis set. For the following examples, the exchange correlation was treated within the generalized gradient approximation according to Perdew and Wang [22]. The k-space integrals over the Brillouin zone were approximated through summation over Monkhorst–Pack special points [23]. Depending on the system under consideration grids of a size between $8 \times 8 \times 8$ and $18 \times 18 \times 18$ were necessary to reach convergence for observables like, for example, formation energy or heat of adsorption. Different super-cells with periodic boundary conditions were constructed to compute bulk, surface and interface properties. For example, the surface of CoAl(111) had to be simulated by a periodic arrangement of symmetric slabs of 19 atomic layers separated by vacuum slabs equivalent to a thickness of 17 layers. Depending on the system and the accuracy demanded the structural optimization was stopped when the forces were below 0.01–0.05 eV Å^{-1}. When necessary, spin-polarized calculations were performed. Of course, for the comparison with the LEED results full geometric relaxations were allowed as also important to study the stability of individual systems.

3. Surface termination of CoAl(111)

The chemical termination of alloy surfaces has been an issue in structural surface science for a long time. Apart from basic research aspects, it is important because of the surface's influence on, for example, the material's catalytic or corrosion properties.

Surface segregation, i.e. the deviation of the stoichiometry in the near surface region from that of the bulk, is usually expected to happen in substitutional disordered alloys due to the generally rather small difference between homogeneous and heterogeneous and atomic bonds (small formation energy). Consistently, for strongly ordering alloys it has long been assumed that there is no segregation of atoms to the surface at all. Important examples which show that the opposite can be true are the B2 phases of NiAl and CoAl. Their bulk formation enthalpies are rather large, namely -0.55 eV/atom [24] and -0.64 eV/atom [25], respectively, as experimentally determined, in excellent agreement with our DFT calculations (-0.57 eV/atom for NiAl, -0.66 eV/atom for CoAl [26]).

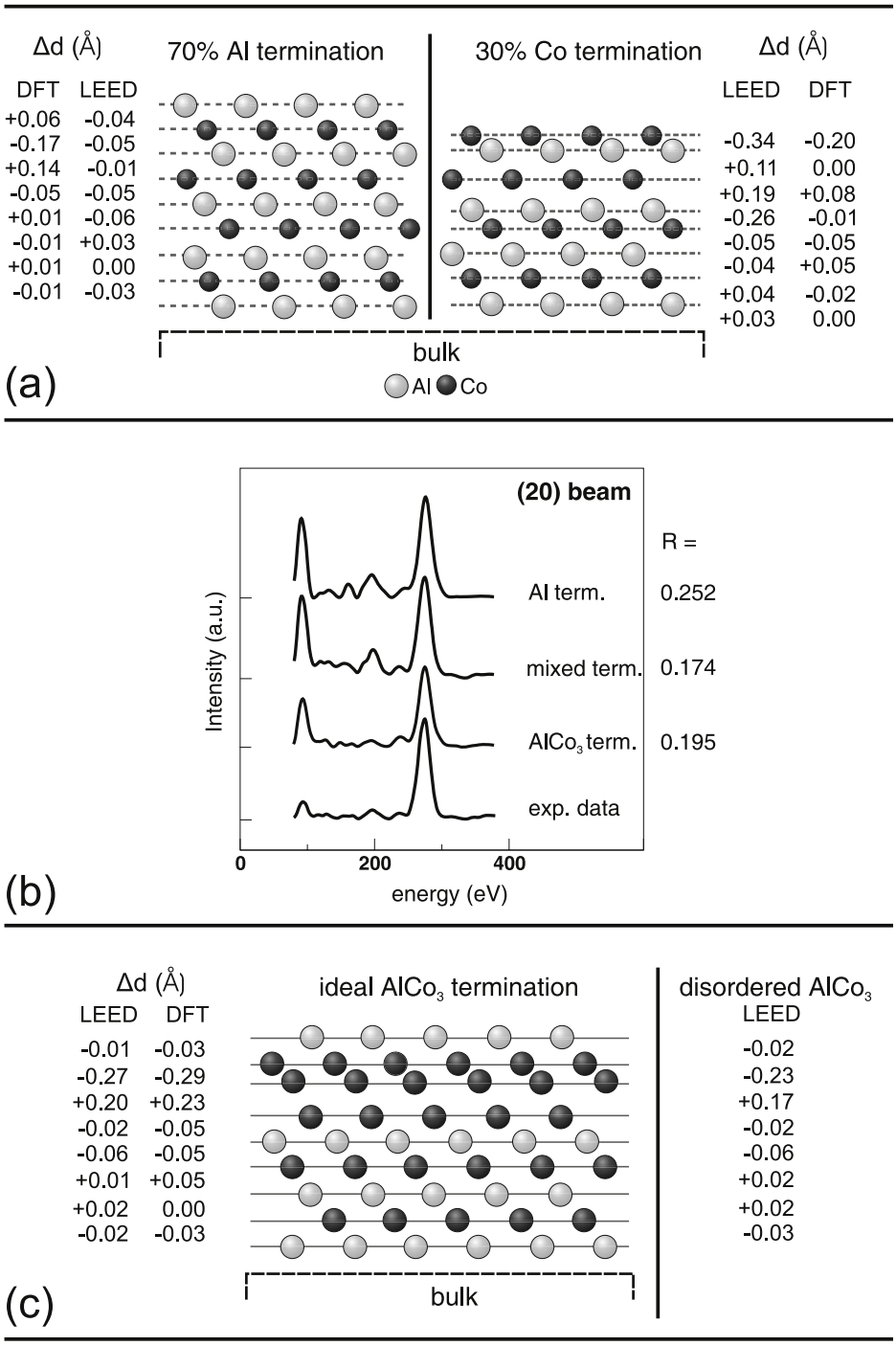

Figure 1. LEED and DFT results of the structural investigation of CoAl(111). The quantity Δd denotes the deviation from the bulk spacing, $d_b = 0.862$ Å. In (a) no surface segregation was allowed, leading to a mixed termination as the best LEED fit. In (c) segregation was allowed resulting in an $AlCo_3$-like termination (see text). Panel (b) compares for the (20) beam the best-fit spectra (including that of single Al termination) with the experimental data. The best-fit R-factors displayed on the right are averages over all beams.

These intermetallics exhibit—according to their B2 structure—alternating elemental layers both in (100) and (111) surface orientation. Consequently, at the surface, the system has only the 'choice' of which of the chemical layers to terminate. Due to the assumption of absent surface segregation, early LEED structure determinations focused on determining the surface termination on the basis of chemically pure and alternating elemental layers. So, they found the NiAl(100) surface to be Al terminated [27, 28] and, surprisingly, NiAl(111) was reported to exhibit coexisting domains with Al and Ni termination (*mixed termination*) [29–31].

For CoAl(111) we also found that a mixed termination leads to a much lower R-factor ($R = 0.174$ [32, 33]) than single termination ($R = 0.252$ for pure Al and $R = 0.361$ for pure Co termination [32]). As indicated in figure 1(a), the weights resulting from the fit are 70% and 30% for Al and Co

terminated domains with, in particular in the Co terminated domain, considerable relaxations of layer spacings involved (note that the bulk layer spacing in the rather open (111) surface is as small as $d_b = 0.862$ Å). In view of the rather low R-factor one could be convinced that the mixed termination model together with the resulting layer relaxations corresponds to the correct surface structure. Yet, inspection of the bond length modifications due to the substantial layer relaxations raises some doubts: so, in the Co terminated (minority) domain the nearest neighbour bond length between Al atoms in the fourth layer and Co atoms in the seventh layer is only 2.13 Å which is unacceptably reduced compared to the bulk value for nearest neighbours (2.48 Å). The doubts turn to certainty when the layer relaxations retrieved by LEED for the two domains are compared with results from DFT as also included in figure 1(a). Even for the top spacing in the two domains, for which LEED usually has the highest sensitivity and lowest statistical error limits (about 0.05 Åin the present case), there is substantial disagreement with the DFT results clearly beyond the error limits.

This is a clear indication that the basis of the LEED structure determination (no surface segregation) is not met in the experiment. We therefore allowed for such segregation—in spite of the high formation enthalpy of Co–Al. We allowed for pure elemental layers of arbitrary sequence with the bulk-like B2 stacking assumed only below the eighth layer (this corresponds in total to $2 \times 2^8 = 512$ different stackings). The best-fit results to be an $AlCo_3$-like termination as displayed in figure 1(c). The R-factor ($R = 0.195$) is not as low as for the mixed termination but is considerably lower than for single termination. Also, the relative intensities compare significantly better to experiment, in particular in the region around 200 eV. To check for the validity of this model we took it as input for a DFT calculation. As displayed on the left-hand side in figure 1(c) the computed layer spacings compare very favourably with those determined by LEED, i.e. within 0.02 Å for the first few spacings and no larger than 0.04 Å throughout the surface. These values are well within the error margins of the two methods.

Yet, two issues concerning the $AlCo_3$ model remain to be clarified. The first is why there can be surface segregation at all in the case of a strongly ordering alloy. As investigated in detail recently [33], the reason behind the phenomenon is the existence of a very tiny off-stoichiometry (surplus of Co) in the material's bulk. Such antisites are energetically very unfavourable in the bulk with the energy cost being as high as 1.29 eV/antisite. So, their existence can only be due to some off-stoichiometry produced during imperfect growth of the alloy or by sample preparation with preferential sputtering and subsequent annealing involved. It turns out that the exchange of such bulk Co antisites with undercoordinated Al atoms in the surface slab is energetically rather favourable. The maximum energy gain (0.80 eV/antisite) is by exchange with third-layer Al atoms in a B2 stacked and Al terminated crystal leading to the described $AlCo_3$ model. So, at the elevated temperatures provided during sample preparation the $AlCo_3$ termination develops by diffusive exchange of atoms. Similar features have also been found for CoAl(100) [34, 35] and NiPt(111) [36].

The second issue to be clarified is the circumstance that the R-factor for the mixed termination model is lower (though only slightly) than that for the $AlCo_3$ terminated crystal. One can argue that this is an artificial result due to the larger number of fit parameters. Yet we felt that it is still a cause for concern and therefore refined the LEED analysis by allowing for some off-stoichiometry in the top three layers which has to be expected anyway in segregation systems. The corresponding structural search, using chemical Tensor LEED [11] based on the average t-matrix approximation (ATA), retrieves a pure Al top layer and the second (third) layer containing 15% (30%) Al instead of consisting of pure Co. Because of the substantial off-stoichiometry in the third layer we also allowed for element-specific sites in that layer, resulting in a layer buckling of 0.10 Å. The resulting best-fit R-factor is $R = 0.172$, i.e. nearly identical to the value obtained for mixed termination. On the right-hand side of figure 1(c) the layer spacings retrieved for this disordered $AlCo_3$ termination are displayed.

4. Hydrogen adsorption

The experimental detection of hydrogen adsorbed on a surface has always been a difficult task. The most sensitive method is the scattering (diffraction) of light atoms, in particular He atom scattering (HAS), by which the surface corrugation corresponding to the adsorption phase can be determined with high precision. Yet it is only by—the non-trivial—interpretation of the measured corrugation that information about the adsorption site and (possibly) the bond length can be retrieved [37]. In quantitative LEED hydrogen enters the scenario only by its rather weak scattering contribution and it is only in special cases that the position of the hydrogen atoms can be retrieved. The simplest case is when no superstructure is involved, so that the substrate responds upon adsorption only by the modification of a few layer spacings. Then the number of structural parameters is still small enough to determine the hydrogen position. Yet even then one needs to know the hydrogen coverage, e.g. whether one or two (or even more) H atoms reside in the surface unit cell. A more difficult scenario is that when hydrogen forms a superstructure with respect to the structure of the uncovered surface. Then the modifications of the substrate follow the superstructure's symmetry and so add to the intensities of superstructure spots. Only when the superstructure induced in the substrate is weak enough so that its intensity contributions are comparable to those of the hydrogen atoms can the latter's positions be determined. In the case of a strong induced substrate reconstruction the contributions from hydrogen scattering remain hidden in that of the substrate, as they can easily be simulated by tiny modifications in the positions of substrate atoms. The same is true when hydrogen adsorbs on an already strongly reconstructed substrate (for reviews see [4, 5]).

In the following we present two examples for the cases described, namely for the simplest case with no superstructure involved but unknown coverage and the most complex case with a strong substrate reconstruction involved. In both cases it is only by the joint application of LEED and DFT that the correct adsorption structure can be retrieved. We choose the

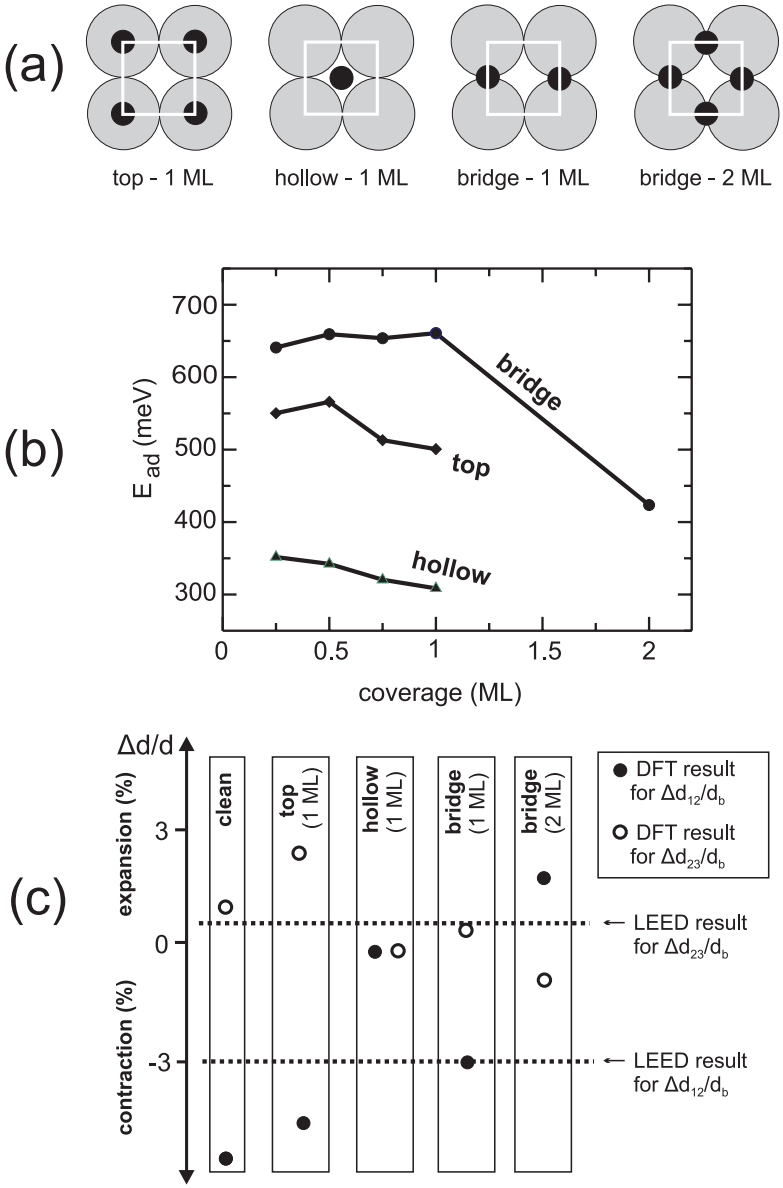

Figure 2. (a) Possible models for the adsorption of H on Ir(100)-(1 × 1). (b) Zero-point corrected average heat of adsorption per H atom calculated by DFT as function of coverage for different adsorption sites. (c) Relative relaxations of the substrate's first two interlayer spacings as calculated by DFT for the clean and hydrogen covered surface for the different adsorption phases displayed in panel (a). The horizontal broken lines give the relaxations resulting from LEED independent of the adsorption phase assumed in the analysis.

Ir(100) surface as a substrate for both examples as it can be prepared both as a (metastable) (1 × 1) phase [38–40] and as its stable phase Ir(100)-(5 × 1)-hex, whose surface is heavily reconstructed exhibiting a quasihexagonally close packed top layer [41, 42].

4.1. Hydrogen on Ir(100)-(1× 1)

The unreconstructed Ir(100) surface was exposed to 100 L H_2 at room temperature (1 L = 10^{-6} Torr s ≈ 1.33 × 10^{-4} Pa s). Upon adsorption the (1 × 1) symmetry of the LEED pattern of the clean surface did not change. In the LEED analysis hydrogen scattering was included whereby the adatoms were allowed to reside in high-symmetry sites as hollow (h) or on-top (t) sites (1 ML coverage in each case) or bridge sites (b) with coverage values of 1 and 2 ML possible (figure 2(a)). It appears that the best-fit R-factors for these structures are $R_h = 0.148$, $R_t = 0.144$, $R_b^{2ML} = 0.120$ and $R_b^{1ML} = 0.101$ with, in the latter case, two orthogonal and equally weighted domains considered and the variance of the R-factor being var(R) = 0.013 [43]. The interlayer spacings in the substrate are practically identical for the four cases.

In view of the small value of the R-factor variance one is tempted to discard all adsorption phases except the bridge site occupation at 1 ML coverage. Yet, even without any consideration of hydrogen scattering evaluation of the LEED data produces a best-fit R-factor as low as $R_0 = 0.111$. So, even a clean surface (with the hydrogen-induced multilayer relaxation considered) is within the error limits, i.e. LEED cannot safely differentiate between a clean surface and a

surface covered with 1 ML hydrogen in bridge sites. This might be taken as a warning to rule out the 2 ML phase with the adatoms also in bridge sites, in particular as the corresponding R-factor is close to the edge of the variance level.

We therefore applied DFT calculations for the adsorption system. In order to get a feeling for the importance of H–H interaction we calculated the heat of adsorption E_{ad} at coverage values of 0.25, 0.5, 0.75, 1 and 2 ML using a (2×2) unit cell. Corrections for zero-point vibrations were included. Figure 2(b) displays E_{ad} per H atom for the three different adsorption sites. Evidently, the bridge site is by far the most favourable. Up to 1 ML coverage (at which $E_{ad} = 661$ meV/atom) there is little influence of H–H interaction on the adsorption energy. Above 1 ML, that is when the second kind of bridge site starts to be occupied, a steep decrease of E_{ad} to 423 meV/atom develops. This is because the heat of adsorption for an additional H atom in the second bridge site (with all the other bridge sites already occupied) is only 185 meV/atom. This might be an indication for hydrogen adsorption beyond 1 ML being improbable at room temperature but cannot be taken as a strict proof.

A reliable decision about the saturation coverage at room temperature comes by comparison of the LEED and DFT results for the *substrate structure* as induced by the hydrogen atoms adsorbed. Independent of the adsorption sites assumed, the best-fit structures of the LEED analyses exhibit a relative contraction of the first substrate spacing by $\Delta d_{12}/d_b = -3.1\%$ and an expansion of the second spacing, $\Delta d_{23}/d_b = +0.5\%$ (note that $\Delta d_{ik} = d_{ik} - d_b$ with d_{ik} the spacing between layers i and k and d_b the bulk value $d_b = 1.924$ Å). Within the error limits of LEED ($\pm 0.5\%$) this pair of values is reproduced by the DFT calculations only for the bridge site phase at 1 ML coverage as illustrated in figure 2(c). Evidently, the substrate's structure as determined by LEED can be used as a fingerprint to identify the correct adsorption phase from the sequence of phases calculated by DFT, that is, only by the mutual interplay of the two methods is the structural problem solved beyond any doubt. The structure is completed by hydrogen's adsorption height in the bridge site which results from DFT as $d_H = 1.178$ Å. The LEED result (1.23 Å) agrees with that within the error limits which, due to the weak scattering of hydrogen, are rather large (0.1 Å).

4.2. Hydrogen on Ir(100)-(5 × 1)-hex

In its ground state the Ir(100) surface is quasihexagonally reconstructed, as has been known for a long time [41]. A close packed surface layer is followed by layers of quadratic order whereby the geometric misfit causes both a (5×1) superstructure (Ir(100)-(5×1)-hex) as well as serious layer bucklings down to at least the fifth layer [42]. By adsorption of hydrogen and simultaneous or subsequent activation by annealing ($T > 180$ K) the hexagonal top layer recovers quadratic order by expelling its extra 20% of atoms to a new surface layer in which they form ordered atomic chains again in five-fold periodicity (Ir(100)-(5×1)-H [44]). Without annealing, the top layer remains in a close packed arrangement ((5×1)-hex-H) as a metastable state and precursor state for the (5×1)-hex→ (5×1)-H phase transition [45].

As shown earlier [45] the LEED intensities of the (5×1)-hex-H phase differ drastically from those of the uncovered surface (5×1)-hex. As a consequence, and because of the weak hydrogen scattering, these strong modifications of the spectra must be dominated by hydrogen-induced changes of atomic positions in the substrate. As the latter's structure is rather complex (with as much as 17 structural parameters involved for the clean surface [42]) there is little or no chance at all to detect the hydrogen positions within the (5×1) unit cell. One the other hand, the negligible contribution of hydrogen scattering pays us back by allowing us to determine the positions of substrate atoms rather accurately.

So, the retrieval of hydrogen positions must come by application of an additional method. Again we applied DFT to the system, not without previously proving that it reproduces the structural parameters determined by LEED for the clean surface with high accuracy [46]. Yet application of DFT to the (5×1)-hex-H phase suffers from the fact that the hydrogen coverage is unknown: even the demanding calculation of the saturation coverage by DFT (the H_2 dissociation must be considered) would not help because the coverage realized in experiment is affected by desorption induced by the electron beam. The solution to this problem comes by using the substrate structure retrieved by LEED as an identifier for the experimentally applied coverage: only for the real coverage and the corresponding correct adsorbate positions will DFT reproduce the substrate structure found by LEED.

By this combined application of DFT and LEED it is found that 0.6 ML of hydrogen atoms are adsorbed, that is, three atoms per (5×1) unit cell as displayed in figure 3. Hollow sites are largely favoured over other sites, though there are small displacements off the ideal hollow sites due to H–H interaction [46]. As a consequence of three adatoms residing in hollow sites the mirror symmetry of the clean surface (indicated by the broken line in the left-hand panels) must be broken by H adsorption, as was indeed found in the LEED analysis [45] (there is, however, a second energetically equivalent domain according to the mirror symmetry of the clean surface, and so the corresponding calculated spot intensities have to be averaged prior to comparison to experiment). This makes the number of model parameters increase to as much as 33. For 27 of them the deviation between the LEED and DFT result is no larger than 0.02 Å, the maximum deviation in the first (second) Ir layer is 0.03 (0.04) Å. Hydrogen induces substrate atoms to shift (at most by about 0.1 Å for atom number 2′) as indicated in the lower right panel of figure 3, enough to modify the intensity spectra of the clean surface substantially as observed experimentally.

5. Interface structure of B2-FeSi films grown on Si(111)

The silicide FeSi in its stable bulk phase (ϵ-FeSi) is semiconducting (though with a very small band gap of 0.05 eV) and owns cubic symmetry with, however, the rather complex B20 structure. Yet, as known for a while [47], the material can also be stabilized as films of the simple B2 structure when

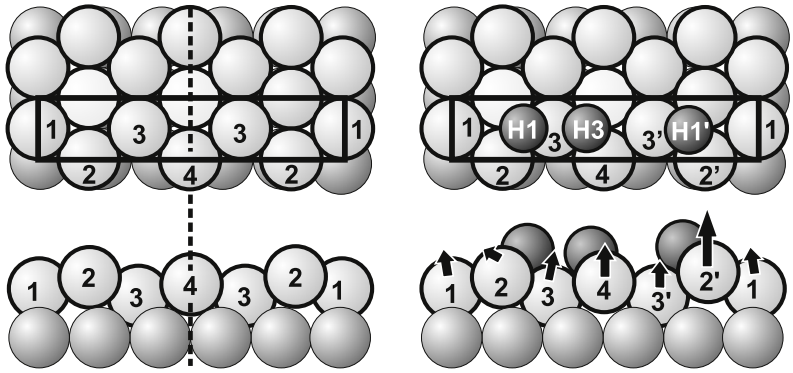

Figure 3. Structure of the clean (left) and hydrogen covered (right) surface Ir(100)-(5 × 1)-hex in on-top view (upper panels) and side view (lower panels); large spheres correspond to the top two Ir layers. The H atoms (small spheres) reside near hollow sites (H). The arrows in the lower right panel (not scaling with the layer spacing) indicate the amount and direction of the displacements of top layer Ir atoms as induced by the adatoms (note that the displacements are <0.1 Å and so are too small to show up for most of the atoms).

epitaxially grown on the unreconstructed Si(111) surface to which it has a lattice mismatch of only 1.5%. It has also been shown that the films consist of (111) oriented layers and that they are terminated by a silicon layer with no other adlayers involved [48]. In the B2 phase FeSi is metallic, so that it forms a Schottky contact with the semiconducting substrate. Because of the corresponding technological relevance we found it interesting and important to know the structure of this FeSi–Si interface.

In order to allow LEED electrons to access the interface we prepared rather thin FeSi films. This was by deposition of about 2.4 ML Fe on the Si(111)-(7 × 7) surface at room temperature. Subsequent annealing lifts the substrate's (7 × 7)-reconstruction with two domains of silicide films of different thickness formed. The thicker (thinner) one is of 40% (60%) weight and their height difference as determined by STM agrees—within the limits of errors—with the step height of the silicide's (111) FeSi double layers (1.6 Å) [49]. So, the two domains will be chemically terminated in the same way whereby, as proven for thicker films, Si termination can be safely assumed. Accordingly, there is a silicide domain of 60% weight with two Fe layers and a domain of 40% weight with three Fe layers which in total make up the 2.4 ML Fe deposited. So, only two domains must be considered in the LEED analysis (if an amount of Fe close to an integer value n of ML had been deposited one would have run the risk of being forced to deal with three domains containing $(n + 1)$, n and $(n - 1)$ ML). As the lateral width of the domains exceeds the lateral transfer width of the electrons (≈100 Å), as also taken from the STM images [49], the LEED analysis can be done by adding domain intensities according to the domain weights (incoherent superposition) with no need to mix amplitudes within the calculations.

There are several structural possibilities for stacking a B2-FeSi film with (111) oriented layers on the Si(111) substrate. On the one hand the lateral unit cells of film and substrate can be aligned so that the stacking proceeds unfaulted from the substrate (A-type stacking). On the other hand the two unit cells can be rotated by 180° with respect to each other so that there is a stacking fault at the interface (B-type stacking). The two cases are illustrated in the two left panels of figure 4(b). Another differentiation for the interface structure is the coordination of Fe atoms closest to the interface which can be five- , seven- and eight-fold. Again two examples are given in figure 4(b). In total the possibilities for the interface structure can be A5, A7, A8, B5, B7 and B8. They all were tried to fit the experimental intensities whereby all interlayer spacings were varied. The resulting best-fit R-factors are (in sequence of increasing value) $R = 0.159$ (B8), 0.180 (B5), 0.206 (B7), 0.209 (A7), 0.221 (A8) and 0.237 (A5).

As the variance of the R-factor is $\mathrm{var}(R) = 0.027$ one can exclude all interface structures except the B8 and B5 case which differ only by an additional Si layer above the last substrate layer. In view of silicon's weaker scattering strength compared to iron it is understandable that LEED fails to distinguish safely between the two structures (whilst the method is rather sensitive to the stacking sequence [50]). So, identification of the correct interface structure can again only come by an independent method. We applied DFT to find out which of the interface configurations is the most stable one. For this, the calculation of the interfacial energies for the individual interface configurations is necessary. As can be seen from 4(b), the film stoichiometry may differ between the individual terminations (e.g. by one Si layer for B5 versus B8) depending on the interface bonding as well as the surface termination of the film (Fe or Si) so that the chemical potentials of FeSi and Si must be taken into account, as described in [48, 49]. Surprisingly, we find that the interfacial energy of the B8 configuration is about 0.2 eV per unit cell lower then that for the B5 configuration, so that the latter can clearly be ruled out. However, the DFT calculations also yield a similar low interfacial energy for the A8 configuration (as displayed on the left side of figure 4(b)) as for the B8 configuration so that the existence of the former cannot be excluded, especially when temperature comes into play. Here, the results of the LEED structure determination help to find a unique answer about the stabilized interface configuration: as mentioned above, the best-fit R-factor for the A8 configuration amounts to $R_\mathrm{p} = 0.221$ and, therefore, lies outside the resulting variance for the best-fit R-factor of the B8 configuration: $R_\mathrm{p}(B8) +$

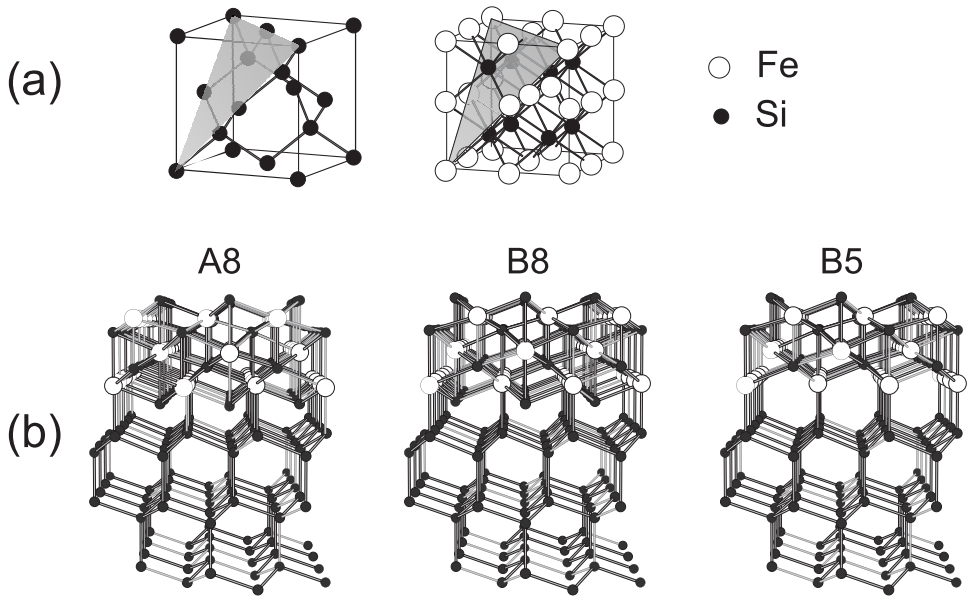

Figure 4. (a) Unit cell of the diamond structure of Si (left) and eight unit cells of B2-FeSi with (111) layers indicated in each case. (b) Examples of the possible interface structures of FeSi(111) films epitaxially arranged on Si(111).

var(R) = 0.154 + 0.027 = 0.181. So, again LEED and DFT agrees perfectly with respect to their most favourable structure (B8), and the second best in each case can be ruled out mutually.

6. Conclusion

As shown by several examples presented above the quantitative determination of surface structures using a single method, LEED or DFT in the present case, can be inhibited by special circumstances like, for example, the presence of very weak scatterers together with strong ones, complex surface reconstructions, unknown coverage of adsorbates, indistinguishability of different models due to an insufficient data base or energetic equivalence. As demonstrated, in such cases the combined application of LEED and DFT can lead to the correct structural solution. Therefore it is not only that one of the methods can distinguish between cases indistinguishable by the other; it may also happen that one method can only work by the input of some partial but safe structural information retrieved by the other method. Moreover, the joint application of an experimentally based method like LEED and a first-principles theoretical method like DFT and comparison of their results mirrors the accuracy of today's surface structure information as they retrieve structural parameters with about the same precision.

References

[1] Watson P R, Van Hove M A and Hermann K 2004 *NIST Surface Structure Data Base, Ver.5.0* (Gaithersburg, MD: National Institute of Standards and Technology)
[2] MacLaren J M, Pendry J B, Rous P J, Saldin D K, Somorjai G A, Van Hove M A and Vvedensky D D 1987 *Surface Crystallographic Information Service* (Dordrecht: Reidel)
[3] Heinz K and Hammer L 2004 *J. Phys. Chem.* B **108** 14579
[4] Heinz K and Hammer L 1996 *Z. Phys. Chem.* **197** 173
[5] Heinz K and Hammer L 1997 *Phys. Status Solidi* a **159** 225
[6] Platow W, Bovensiepen U, Poulopoulos P, Farle M, Baberschke K, Hammer L, Walter S, Müller S and Heinz K 1999 *Phys. Rev.* B **59** 12641
[7] Pendry J B 1980 *J. Phys. C: Solid State Phys.* **13** 937
[8] Döll R and Van Hove M A 1996 *Surf. Sci.* **355** L393
[9] Kottcke M and Heinz K 1997 *Surf. Sci.* **376** 352
[10] Heinz K and Hammer L 1998 *Z. Kristallogr.* **213** 615
[11] Heinz K 1995 *Rep. Prog. Phys.* **58** 637
[12] Rous P J, Pendry J B, Saldin D K, Heinz K, Müller K and Bickel N 1986 *Phys. Rev. Lett.* **57** 2951
[13] Rous P J 1989 *Surf. Sci.* **219** 355
[14] Blum V and Heinz K 2001 *Comp. Phys. Commun.* **134** 392
[15] Pendry J B 1974 *Low Energy Electron Diffraction* (London: Academic)
[16] Kresse G and Furthmüller J 1996 *Comput. Mater. Sci.* **6** 15
[17] Kresse G and Furthmüller J 1996 *Phys. Rev.* B **54** 11169
[18] Vanderbilt D 1990 *Phys. Rev.* B **41** 7892
[19] Kresse G and Hafner J 1994 *J. Phys.: Condens. Matter* **61** 8245
[20] Kresse G and Joubert D 1999 *Phys. Rev.* B **59** 1758
[21] Blöchl P E 1994 *Phys. Rev.* B **50** 17953
[22] Perdew J P and Wang Y 1992 *Phys. Rev.* B **45** 13244
[23] Monkhorst H J and Pack J D 1976 *Phys. Rev.* B **13** 5188
[24] Meschel S V and Kleppa O J 1994 *Metallic Alloys: Experimental and Theoretical Perspectives* ed J S Faulkner and R G Jordan (Amsterdam: Kluwer)
[25] Nash P and Kleppa O 2001 *J. Alloys Compounds* **321** 228
[26] Müller S 2003 *J. Phys.: Condens. Matter* **15** R1429
[27] Davis H L and Noonan J R 1987 *Mater. Res. Soc. Symp.* **83** 3
[28] Davis H L and Noonan J R 1988 *Springer Ser. Surf. Sci.* **11** 152
[29] Noonan J and Davis H 1987 *Phys. Rev. Lett.* **59** 1714
[30] Niehus H 1988 *Nucl. Instrum. Methods* B **33** 876
[31] Overbury S, Mullins D and Wendelken J 1990 *Surf. Sci.* **236** 122
[32] Blum V 2002 *PhD Thesis* Universität Erlangen-Nürnberg
[33] Hammer L, Blum V, Schmidt C, Wieckhorst O, Meier W, Müller S and Heinz K 2005 *Phys. Rev.* B **71** 075413
[34] Blum V, Hammer L, Schmidt C, Meier W, Wieckhorst O, Müller S and Heinz K 2002 *Phys. Rev. Lett.* **89** 266102

[35] Wieckhorst O, Müller S, Hammer L and Heinz K 2004 *Phys. Rev. Lett.* **92** 195503
[36] Pourovskii L V, Ruban A V, Johansson B and Abrikosov I A 2003 *Phys. Rev. Lett.* **90** 026105
[37] Farias D and Rieder K H 1998 *Rep. Prog. Phys.* **61** 1575
[38] Küppers J and Michel H 1979 *Appl. Surf. Sci.* **3** 179
[39] Heinz K, Schmidt G, Hammer L and Müller K 1985 *Phys. Rev.* B **32** 6214
[40] Lerch D, Klein A, Schmidt A, Müller S, Hammer L, Heinz K and Weinert M 2006 *Phys. Rev.* B **73** 075430
[41] Ignatiev A, Jones A and Rhodin T 1972 *Surf. Sci.* **30** 573
[42] Schmidt A, Meier W, Hammer L and Heinz K 2002 *J. Phys.: Condens. Matter* **14** 12353
[43] Schmidt A 2006 *PhD Thesis* Universität Erlangen-Nürnberg
[44] Hammer L, Meier W, Klein A, Landfried P, Schmidt A and Heinz K 2003 *Phys. Rev. Lett.* **91** 156101
[45] Poon H C, Saldin D K, Lerch D, Meier W, Schmidt A, Klein A, Müller S, Hammer L and Heinz K 2006 *Phys. Rev.* B **74** 125413
[46] Lerch D, Müller S, Hammer L and Heinz K 2006 *Phys. Rev.* B **74** 075426
[47] von Känel H, Mäder K A, Müller E, Onda N and Sirringhaus N 1992 *Phys. Rev.* B **45** 13807
[48] Walter S, Bandorf R, Weiß W, Heinz K, Starke U, Strass M, Bockstedte M and Pankratov O 2003 *Phys. Rev.* B **67** 85413
[49] Walter S, Blobner F, Krause M, Müller S, Heinz K and Starke U 2003 *J. Phys.: Condens. Matter* **15** 5207
[50] Ascolani H, Cerda J R, de Andres P L, de Miguel J J, Miranda R and Heinz K 1996 *Surf. Sci.* **345** 320